01 Jan 2003

Mechanical Property Characterization of Mouse Zona Pellucida

Yu Sun

Kai-tak Wan
Missouri University of Science and Technology

K. P. Roberts

J. C. Bischof

et. al. For a complete list of authors, see https://scholarsmine.mst.edu/mec_aereng_facwork/3373

Mechanical Property Characterization of Mouse Zona Pellucida

Yu Sun*, *Member, IEEE*, Kai-Tak Wan, Kenneth P. Roberts, John C. Bischof, and Bradley J. Nelson, *Member, IEEE*

Abstract—**Previous intracytoplasmic sperm injection (ICSI) studies have indicated significant variation in ICSI success rates among different species. In mouse ICSI, the zona pellucida (ZP) undergoes a "hardening" process at fertilization in order to prevent subsequent sperm from penetrating. There have been few studies investigating changes in the mechanical properties of mouse ZP post fertilization. To characterize mouse ZP mechanical properties and quantitate the mechanical property differences of the ZP before and after fertilization, a microelectromechanical systems-based multiaxis cellular force sensor has been developed. A microrobotic cell manipulation system employing the multiaxis cellular force sensor is used to conduct mouse ZP force sensing, establishing a quantitative relationship between applied forces and biomembrane structural deformations on both mouse oocytes and embryos. An analytical biomembrane elastic model is constructed to describe biomembrane mechanical properties. The characterized elastic modulus of embryos is 2.3 times that of oocytes, and the measured forces for puncturing embryo ZP are 1.7 times those for oocyte ZP. The technique and model presented in this paper can be applied to investigations into the mechanical properties of other biomembranes, such as the plasma membrane of oocytes or other cell types.**

Index Terms—**Biomembrane mechanical modeling, elastic modulus, force sensing, intracytoplasmic sperm injection (ICSI), microelectromechanical systems (MEMS), microrobotic cell manipulation, zona pellucida (ZP) hardening.**

I. INTRODUCTION

INVESTIGATIONS into the functions and behaviors of various biological structures often require that the biomembranes[1] isolating these structures from their immediate surroundings are characterized. The most common biomembranes are those composed of lipids and proteins, such as plasma membranes. Membrane lipids are organized in a bilayer that has two closely opposed sheets. Embedded in and associated with the lipid portion of the membrane are proteins. There are other types of biomembranes that have compositions different than lipid bilayer membranes. For example, the zona pellucida (ZP) is an extracellular biomembrane enveloping an oocyte. It is composed of three sulfated glycoproteins called ZP-1, ZP-2, and ZP-3 that are synthesized by the oocyte [1].

[1]In this paper, *biomembrane* refers to sheetlike structures surrounding cells.

Upon fertilization, the ZP surrounding the oocyte undergoes a "hardening" process in order to prevent subsequent sperm from penetrating. It has been speculated that ZP hardening is due to glycoprotein modification after fertilization. In cortical reactions occurring after fertilization, cortical granules undergo exocytosis as a result of an increase in the level of calcium, which modifies ZP glycoproteins resulting in ZP hardening [2]. Some researchers deduce that the conversion of the ZP glycoprotein ZP-2 to ZP-2f specifically contributes to ZP hardening [3]. ZP hardening has been assessed by comparing the duration of zona lysis in the presence of alpha-chymotrypsin [4]. However, there have been few studies investigating changes in the mechanical properties of the ZP post fertilization.

To better understand the mechanical properties of mouse ZP and the mechanical property differences of ZP before and after fertilization, biomembrane force sensing has been conducted on mouse oocytes and embryos using a novel two-axis cellular force sensor [5]. A biomembrane mechanical model has been proposed to describe the mechanical properties of the ZP. Consequently, a quantitative relationship between applied forces and biomembrane structural deformations on both mouse oocytes and embryos is established, and ZP hardening is quantitated. The technique and model presented here can be applied to mechanical property investigations of other biomembranes, such as the plasma membrane of oocytes or other cell types.

In this paper, the cell preparation process used for obtaining mouse oocytes and embryos is introduced in Section II. The microelectromechanical systems (MEMS)-based two-axis cellular force sensor used to measure forces applied to cells is described in Section III. The microrobotic cell manipulation system setup is presented in Section IV. The experimental results on mouse oocyte and embryo membranes are discussed in Section V. The biomembrane mechanical model is described in Section VI. Section VII presents the determined elastic modulus of mouse oocyte and embryo ZP. Results are discussed in Section VIII. The paper concludes in Section IX.

II. CELL PREPARATION

The mouse oocytes and embryos used in the experiments were collected in accordance with standard established procedures [6]. Briefly, three week old FVB/N female mice were injected with pregnant mare serum (PMS) to promote follicular recruitment maturation. After approximately 45 h, the mice were injected with human chorionic gonadotropin (hCG) to stimulate synchronized ovulation. Approximately 40 oocytes were collected from the ampulla of female mice. To collect embryos, superovulated female mice were mated to fertile male mice. Approximately 40 embryos were collected. The
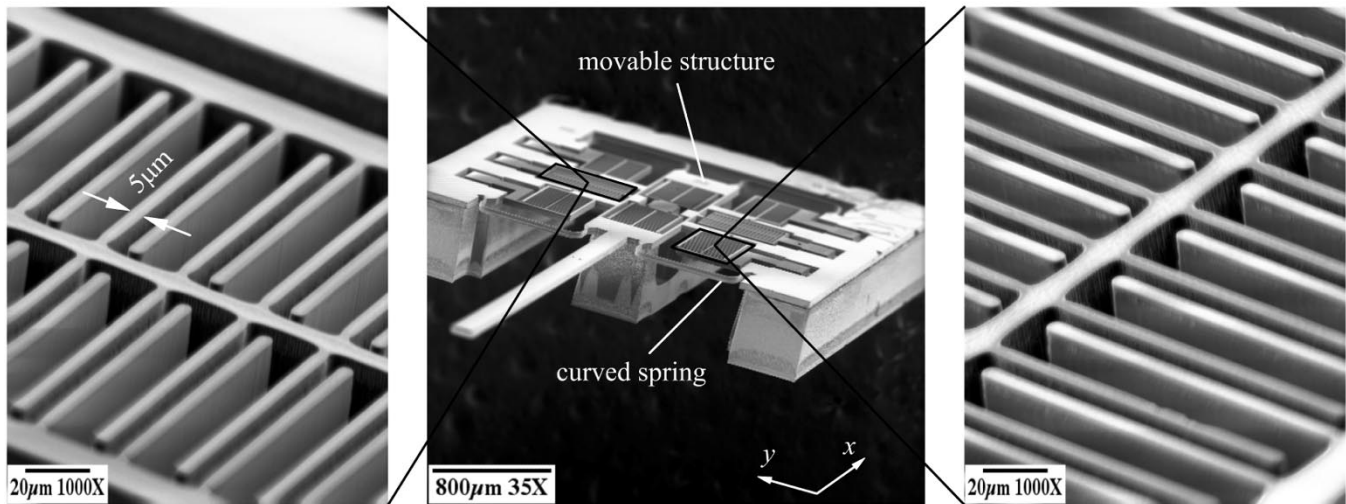
Fig. 1.   Scanning electron microscopy image of a cellular force sensor with orthogonal comb drives detailed.
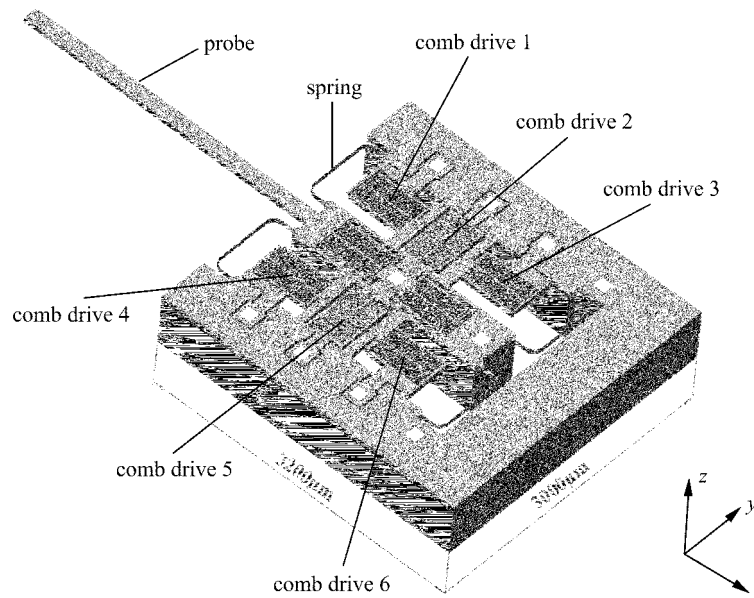

Fig. 2.   Solid model of the multiaxis cellular force sensor.

diameters of the collected oocytes and embryos varied from 52 to 61 μm.

III. MEMS-BASED MULTIPLE-AXIS CAPACITIVE CELLULAR FORCE SENSOR

The MEMS-based two-axis cellular force sensor [5] shown in Fig. 1 is capable of resolving normal forces applied to a cell as well as tangential forces generated by improperly aligned cell probes. A high-yield microfabrication process was developed to form the three-dimensional high aspect ratio structure by using deep reactive ion etching (DRIE) on silicon-on-insulator (SOI) wafers.

As shown in Fig. 2, the constrained outer frame and the inner movable structure are connected by four curved springs. A load applied on the probe causes the inner structure to move, changing the gap between each pair of interdigitated comb capacitors. Consequently, the total capacitance change resolves

the applied force. The interdigitated capacitors are orthogonally configured to make the force sensor capable of resolving forces in both the x and y directions. The cellular force sensors used in the experiments have spring widths of 3 and 5 μm, which are capable of resolving forces up to 25 μN with a resolution as low as 0.01 μN.

IV. MICROROBOTIC CELL MANIPULATION SYSTEM

The microrobotic cell manipulation system is composed of the capacitive cellular force sensor, a cell holding unit, a vacuum unit, an imaging unit and a software unit, as shown in Fig. 3.

For cellular force measurement vibration must be well controlled because vibration affects measurement accuracy. To minimize vibration, all units except the host computer are mounted on a vibration isolation table.

The cellular force sensor, wire bonded to a readout circuit board, is mounted on a three degrees-of-freedom (DOF) micro-
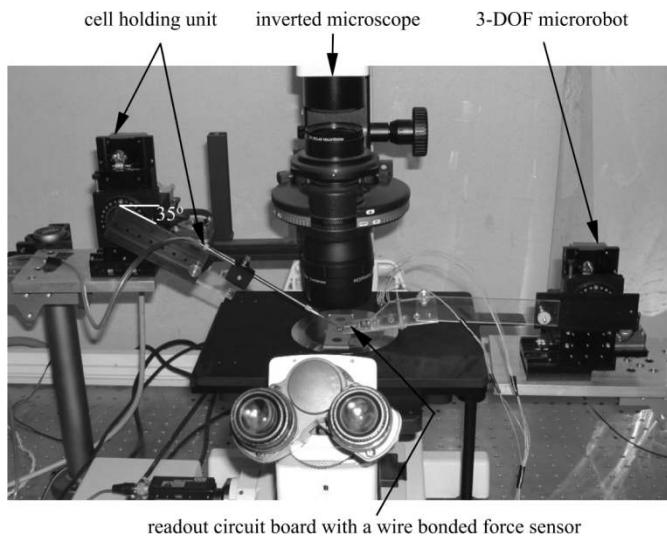
cell holding unit   inverted microscope   3-DOF microrobot

readout circuit board with a wire bonded force sensor

Fig. 3.   Biomanipulation system setup for biomembrane force sensing.
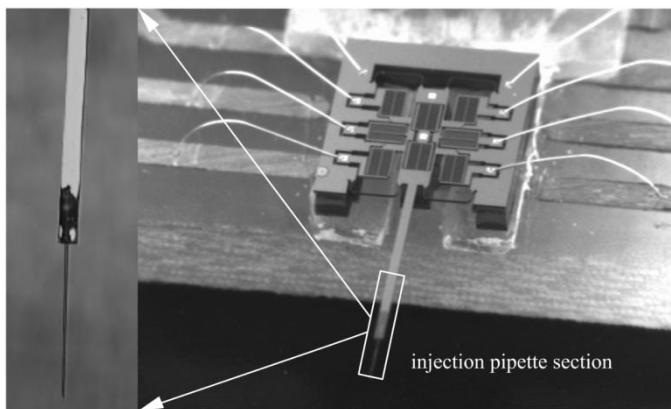
injection pipette section

Fig. 4.   Wire-bonded force sensor with an attached injection pipette section.

robot, in which the XYZ axes each has a travel of 2.54 cm with a step resolution of 40 nm.

Tip geometry effects the quantitative force measurement results. To obtain valid biomembrane force information for intracytoplasmic sperm injection (ICSI) studies, a standard ICSI injection pipette (Cook K-MPIP-1000–5) tip section with a tip diameter of 5 μm is attached on the probe tip of the cellular force sensors, as shown in Fig. 4.

The cell holding unit of the system includes a 3-DOF microrobot and a standard pipette holder with a bent ICSI holding pipette (Cook K-HPIP-1035–5; bending angle 35°). The dimensions of the holding pipette tips are 15 μm in inner diameter and 75 μm in outer diameter.

A voltage-controlled Venturi vacuum generator capable of producing up to 15 inches Hg (inHg) vacuum was developed for this study. The calibrated relationship between the applied voltage and the resulting pressure is linear, given as $P = 8.1 \, V_{\text{applied}} - 14.7$, where P denotes pressure in inHg, and V_{applied} is in volts. In the experiments, a 5.5-inHg sucking pressure (corresponding to a V_{applied} of 2.5 V) is consistently applied for cell fixation.

bent holding pipette

force sensor probe with an injection pipette section attached

vacuum

35°

d

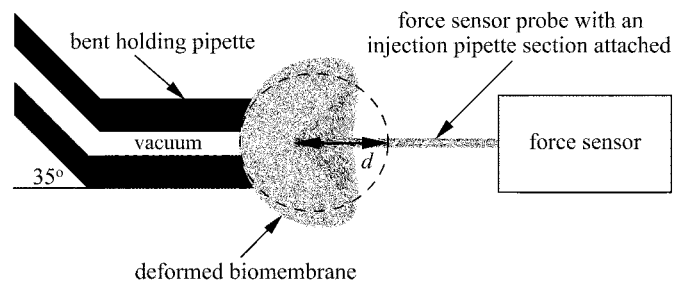force sensor

deformed biomembrane

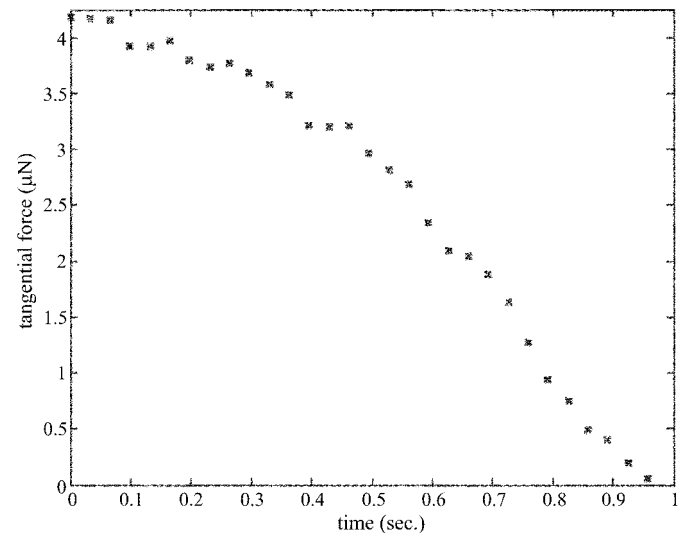Fig. 5.   Force–distance measurement system configuration (not to scale).

Fig. 6.   Tangential force change during probe alignment.

The system configuration under the microscope is shown in Fig. 5. The bent holding pipette tip, the cell, and the force sensor probe are horizontally aligned.

The imaging unit includes an inverted microscope, a charge-coupled device (CCD) camera, a peripheral component interconnect (PCI) frame grabber, and a host computer. A Nikon TE200 inverted microscope is used with a 40× long working distance objective and a Hoffman modulation contrast condenser. The CCD camera is mounted on the side port of the microscope. The frame grabber captures 30 frames/s.

The software unit samples the cell membrane deformation images and forces synchronously. The membrane geometries in each frame of image are measured offline with a resolution of one pixel.

V. EXPERIMENTAL RESULTS

The mouse oocytes and embryos incubated in human tubal fluid (HTF) were individually transferred into modified HTF (mHTF), containing the Hepes buffer, for the force sensing experiments. Before the force sensor applies a uniaxial point load compressing the biomembrane and measures normal forces, the force sensor probe must be properly aligned such that tangential forces are minimized. This ensures that only a normal force is applied to the membrane. Fig. 6 shows the tangential force
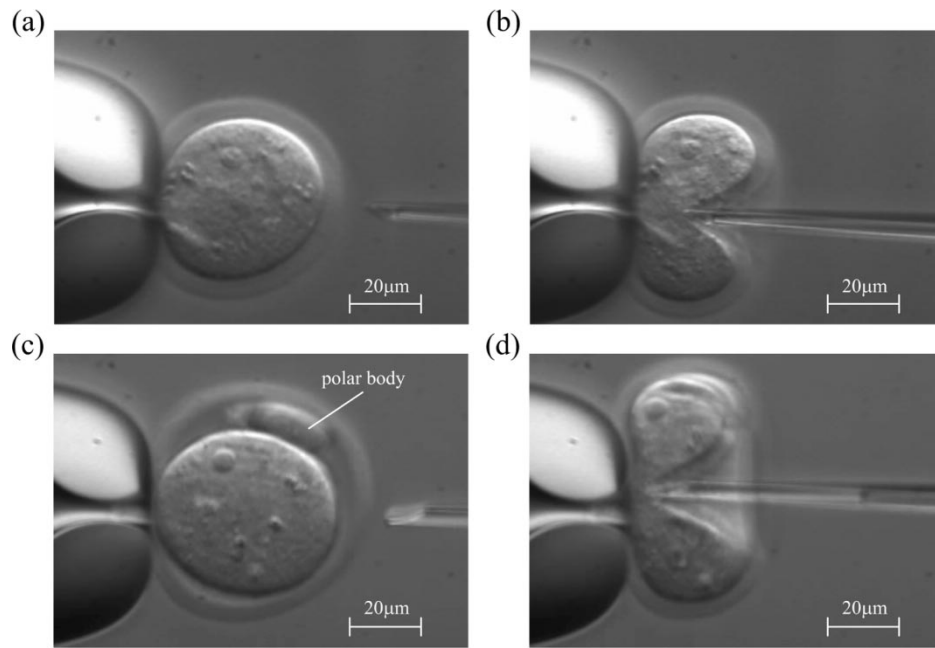
Fig. 7.   Force-deformation curve measurement. (a) and (b) Mouse oocyte ZP. The applied force is 7.21 μN, and the indenter displacement is 42.2 μm. (c) and (d) Mouse embryo ZP. The applied force is 12.7 μN, and the indenter displacement is 52.3 μm.

change on a mouse embryo ZP captured during the probe alignment process. When the tangential force is minimized, normal forces and membrane geometry changes are captured.

A. Mouse Oocyte ZP Experiments

Fig. 7(a) and (b) show the force and deformation measurement process on a mouse oocyte ZP. As shown in Fig. 8, where the horizontal axis is membrane deformation denoted as d in Fig. 5, forces increase nonlinearly as deformation increases. When deformation reaches about 45 μm, the ZP and the plasma membrane are punctured, which results in the maximum forces measured, i.e., the puncturing forces. The puncturing forces are approximately 7.5 μN. After the force sensor tip punctures the membranes and travels into the cytoplasm, the force decreases rapidly, almost to zero.

B. Mouse Embryo ZP Experiments

Fig. 7(c) and (d) show the force and deformation measurement process on a mouse embryo ZP. The membranes are deformed as much as 53 μm before being punctured. The puncturing forces are approximately 13 μN, as shown in Fig. 8.

C. Comparison of Experimental Results

Table I summarizes the puncturing forces and largest deformations that occurred on the membranes.

It can be seen that embryo membranes endure much larger deformations than oocyte membranes before being punctured. The required forces to puncture embryo membranes are almost twice as large as the forces for oocyte membranes. These measurement results quantitatively reveal the mechanical property differences that result from mouse ZP hardening. To further investigate biomembrane mechanical properties and biomembrane geometry changes from an applied force, a biomembrane mechanical model is needed.
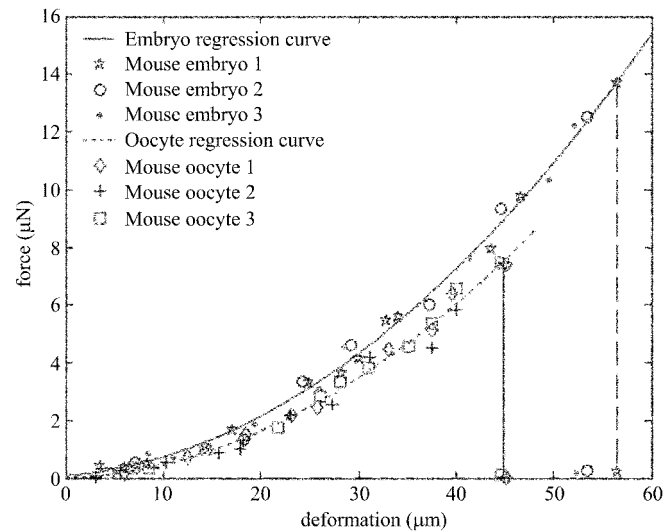
Fig. 8.   Force-deformation curves of mouse oocyte and embryo membranes.

TABLE I
COMPARISON OF THE EXPERIMENTAL RESULTS ON THE BIOMEMBRANES

biomembrane	largest deformation	puncturing force
mouse oocyte ZP	44μm	7.5μN
mouse embryo ZP	53μm	13μN

VI. BIOMEMBRANE MECHANICAL MODELING

A. Existing Biocapsule Elastic Models

The two popular biocapsule models are the contact mechanics models and the micropipette aspiration model. These models are not appropriate to use for describing the mouse ZP loading situations. The contact mechanics models including the Hertzian model [7], [8] and Sneddon model [9], [10] treat

a deformed object as a solid body. Encapsulated biocapsules are by no means solid bodies. Furthermore, dimple depths in the mouse ZP experiments violate the small deformation assumption of the contact mechanics models. Additionally, the contact mechanics models assume shearing and compression exist only in the proximity of the contact area, while the force sensor probe stretches the entire enclosing membrane in the experiments (see Fig. 7). Finally, the contact mechanics models assume there is only a local dimple geometry change and the global geometry of the deformed object remains unchanged, which is not the case in the mouse ZP loading situations. Thus, contact mechanics models are not appropriate to use for revealing the mechanical properties of loaded mouse oocyte and embryo membranes.

To measure mechanical properties of cells, a cell must be deformed in some way by a known force or stress. For example, in the mouse egg cell and embryo experiments, a uniaxial force was applied to indent the cell membranes. Using the micropipette aspiration technique that was originally developed by Mitchison and Swann [11], cell membrane material properties are determined by applying a sucking pressure on the cell membrane through a micropipette and membrane deformation is visually measured.

The elastic model describing the membrane geometry changes and material properties [12] is

$$\Delta P = 2K \frac{\Delta A}{A_0} \left(\frac{1}{R_p} - \frac{1}{R_c} \right) \tag{1}$$

where ΔP is the applied sucking pressure, K is the area elastic modulus, A_0 is the original surface area of the entire membrane, and $\Delta A \approx 2\pi R_p L (1 - R_p/R_c)$ is the outer membrane surface area change in terms of the projection length L and the radii of pipette R_p and the outer membrane R_c. This model has been widely used for characterizing lipid vesicle material properties and in cell adhesion studies [13]–[16].

The micropipette aspiration model describes a different biomembrane deformation situation than the mouse ZP experiments. First, the micropipette model assumes that a sucking pressure is applied to deform a biomembrane while in the mouse oocyte and embryo membrane loading experiments, uniaxial forces are applied on the membranes. Second, the biomembrane deformation mode is different, resulting in different membrane geometries. In the micropipette aspiration model, a biomembrane is elongated in the micropipette while biomembranes were indented in the mouse oocyte and embryo membrane loading situations. Hence, the micropipette aspiration model does not apply in describing the mouse oocyte and embryo membrane loading situations.

B. Biomembrane Point-Load Model

Due to the deficiencies of existing models, a biomembrane point-load model is proposed in this paper, which considers a biomembrane as a thin film and assumes that the inner cytoplasm provides a hydrostatic pressure on the membrane. From experimental observations, the membrane shape can be characterized with three geometric parameters. For a given biomembrane deformed by an indenter, this biomembrane point-load
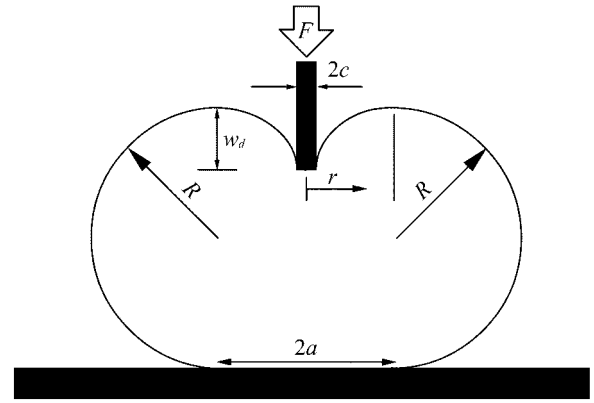

Fig. 9. Indentation of a cell membrane by a micropipette.

model together with the experimental data is capable of characterizing the biomembrane mechanical properties and accurately predicting membrane deformation shape.

Throughout modeling, the following are assumed.

1) The biomembrane encapsulates liquid (i.e., cytoplasm) that exerts a uniform hydrostatic pressure on the biomembrane.
2) The cell volume does not change.
3) The biomembrane has a negligible flexural rigidity, so that deformation is caused by membrane stretching alone.
4) The biomembrane is linearly elastic.
5) The cell is free of initial membrane stress or residual stress.
6) The model starts with a planar circular area with zero residual stress.

The three geometric parameters describing an indented biomembrane shape are a, w_d, and R, as shown in Fig. 9. A micropipette of radius c exerts a force F on the membrane, creating a dimple with radius a and depth w_d and semicircular curved surfaces with radius R. The resultant membrane shape is a reasonable approximation.

In deriving the model, first consider force equilibrium at the local dimple. As shown in Fig. 10, the internal pressure produces a force $\pi r^2 p$ counterbalancing the applied force F, where p is the internal pressure. Another counterbalancing force $\sigma_d \sin \theta 2\pi rh$ is due to the membrane stress σ_d. These two forces together balance the applied force F. For small angle approximations, $dw/dr \approx \sin \theta \approx \theta$, where w is the deformed dimple profile [17]. Thus, the force balance equation at equilibrium is

$$F = \pi r^2 p + \sigma_d 2\pi rh \frac{dw}{dr}$$

or

$$\sigma_d h \frac{dw}{dr} = \frac{F}{2\pi r} - \frac{pr}{2} \tag{2}$$

where h is membrane thickness.

Integrating (2) with a boundary condition of $w = 0$ at $r = a$ and approximating $p = F/(\pi a^2)$ yield the dimple profile

$$w = -\frac{F}{4\pi \sigma_d h} \left[1 - \left(\frac{r}{a} \right)^2 + \ln \left(\frac{r}{a} \right)^2 \right] \tag{3}$$
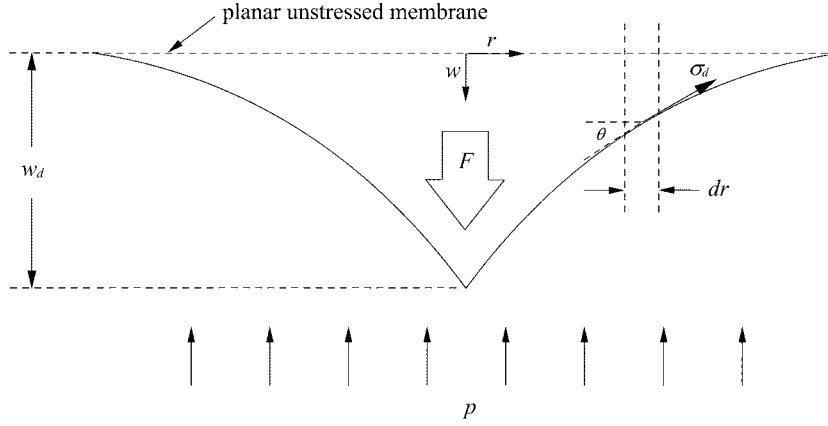
which is valid in $c \leq r \leq a$.

Fig. 10. Force balance and elastic strain analysis at the dimple.

The dimple depth from the maximum height of the deformed membrane, as shown in Fig. 9, is given by

$$w_d = w|_{r=c}$$
$$= -\frac{F}{4\pi\sigma_d h}\left[1 - \left(\frac{c}{a}\right)^2 + \ln\left(\frac{c}{a}\right)^2\right]. \quad (4)$$

Within the dimple, each ring element on the membrane of radius r and width dr is stretched by the external load to a final width of $dr/\cos\theta$, as shown in Fig. 10. If $\theta < 25°$ holds, the small strain approximation is valid. The largest θ in the experiments is less than $22°$. The elastic strain on such an element is, therefore, given by

$$\varepsilon_d = \frac{\frac{dr}{\cos\theta} - dr}{dr}$$
$$\approx \frac{\theta^2}{2}$$
$$= \frac{1}{2}\left(\frac{dw}{dr}\right)^2. \quad (5)$$

Since elastic strain on a membrane is proportional to area change [17], one can ignore the second-order terms, and the average strain on the membrane is

$$\bar{\varepsilon}_d = \frac{1}{2}\frac{\int\limits_c^a \frac{1}{2}\left(\frac{dw}{dr}\right)^2 rdr}{\int\limits_c^a rdr}. \quad (6)$$

Note that the denominator is simply the area of the annulus, with c and a the inner and outer radii, respectively.

Linear elasticity requires [18], [19]

$$\bar{\sigma}_d = \frac{E}{1-\nu}\bar{\varepsilon}_d \quad (7)$$

where E is the membrane elastic modulus and ν is the Poisson ratio.

Combining (4) and (7) yields

$$F = \frac{2\pi Ehw_d^3}{a^2(1-\nu)}\left[\frac{3 - 4\zeta^2 + \zeta^4 + 2\ln\zeta^2}{(1-\zeta^2)(1-\zeta^2+\ln\zeta^2)^3}\right] \quad (8)$$

where $\zeta = c/a$.

Next, the overall biomembrane volume is considered. Before being compressed, the cell is approximately a sphere of radius R_0. The initial volume of the sphere is

$$V_0 = \frac{4}{3}\pi R_0^3. \quad (9)$$

The total volume of the biomembrane shown in Fig. 9 is the subtraction of volume V_t of a filled torus from volume V_d of the local dimple. The volume of a filled torus is

$$V_t = 2\int_R^{2R} \pi x^2 dy$$
$$= \frac{\pi R}{3}\left(6a^2 + 3\pi aR + 4R^2\right) \quad (10)$$

where y is the profile of the curved surface to the right of the y axis and $y = \sqrt{R^2 - (x-a)^2} + R$.

The volume of the local dimple shown in Fig. 9 is

$$V_d = \int_0^{w_d} \pi r^2 dw$$
$$= \frac{\pi w_d}{2}\left[\frac{a^2\left(1-\zeta^2\right)^2}{1-\zeta^2+\ln\zeta^2}\right]. \quad (11)$$

Hence, the volume of the deformed geometry shown in Fig. 9 is

$$V = V_t - V_d. \quad (12)$$

According to volume conservation $V = V_0$ and from (12),

$$4R^3 + 3\pi aR^2 + 6a^2R = 4R_0^3 + \frac{3w_d}{2}\left[\frac{a^2\left(1-\zeta^2\right)^2}{1-\zeta^2+\ln\zeta^2}\right] \quad (13)$$

which relates the three geometric parameters a, w_d, and R.

In the above equations, biomembrane material parameters E and ν and dimensions R_0, h, and c are constants, while geometric parameters a, R, and w_d and applied force F are variables.

In the proposed point-load model, the sucking pressure for cell fixation is not included for several reasons. First, very low sucking pressure (5.5 inHg) was applied in order to minimize the intrinsic stress increase. Second, the small sucking pressure only slightly increased the contact circle dimension at the base.

TABLE II
ELASTIC MODULUS OF MOUSE OOCYTE AND EMBRYO ZP

statistics	oocyte ZP modulus	embryo ZP modulus
mean	17.9kPa	42.2kPa
standard deviation (1σ)	0.8kPa	2.1kPa
relative deviation	4.59%	4.9%

To further minimize this effect, the measurements of the parameter a were conducted on the dimple side instead of at the cell–substrate interface. The major limitation of the model is in the treatment of membrane stress within the dimple, which is not uniform. The adopted method of averaging the elastic strain in the dimple is only a reasonable approximation. Another limitation of the model is that an initial planar circular area with zero residual stress is assumed, which is not the case in reality.

VII. DETERMINATION OF MOUSE ZP ELASTIC MODULUS

The geometric parameters a and w_d are measured from images captured in the experiments. F is the measured force. The Poisson ratio ν of the biomembranes is assumed to be 0.5 [20], [21]. The constant values used are 4.5 μm in ZP thickness (h) and 3 μm in indenter radius (c). Using (8) of the biomembrane point-load model, the Young's modulus of mouse oocyte and embryo ZP is calculated.

Table II summarizes the elastic modulus results, based on 34 data points from three mouse oocytes and 31 data points from three mouse embryos. Throughout the ZP loading process, the modulus values are fairly constant. Elastic modulus values for individual membranes vary only slightly from the values listed in Table II. Quantitatively, the mean elastic modulus of mouse embryo ZP (42.2 kPa) is more than twice that of mouse oocyte ZP (17.9 kPa).

VIII. DISCUSSION

Experimental results demonstrate that the forces for puncturing embryo ZP (13 μN) are almost twice those for oocyte ZP (7.5 μN). The characterized elastic modulus increases from 17.9 kPa for oocyte ZP to 42.2 kPa for embryo ZP. These results quantitatively describe mouse ZP mechanical properties and quantitate ZP hardening. Further research is needed to investigate whether this mechanical property change is caused by a change in protein structure or protein rearrangement, which can be studied using various methods such as Fourier transform infrared spectroscopy (FTIR) [22].

The elastic modulus of various cell types have been reported in the literature. The modulus values span a large range from 1–50 kPa for organelles of human platelets [23], 0.013–0.15 MPa for lung carcinoma cells [24], 0.67 MPa for rat atrial myocytes [25], 4.3 MPa for rat mast cells [26], to 10 MPa for human red blood cells [27]. There has been no reported modulus characterization results on mouse ZP. The characterized mouse ZP modulus values are within this large range of [1 kPa, 10 MPa]. However, they are not directly comparable to the reported modulus values for other cell types because the reported results are based on different techniques and models for lipid-bilayer membranes, while the results presented in this paper are based on the proposed biomembrane point-load model for mouse ZP composed of proteins.

Other techniques that can be used for characterizing mouse ZP mechanical properties include the micropipette suction technique, the atomic force microscopy (AFM) technique, and the magnetic bead force measurement method [28]. Compared to other techniques, the technique presented in this paper uses an experimental setup and conditions consistent with ICSI, thus providing valid measurement results and information on ZP properties particularly relevant for ICSI studies.

IX. CONCLUSION

This paper theoretically and experimentally characterizes the mechanical properties of mouse oocyte and embryo ZP. A two-axis cellular force sensor was integrated into a microrobotic system for biomembrane force sensing. Quantitative force measurement results on mouse oocyte and embryo ZP were obtained. A biomembrane point-load mechanical model was constructed that reveals the resulting geometric changes on biomembranes from an applied force. The Young's modulus of mouse oocyte and embryo ZP was determined. ZP puncturing forces increased from 7.5 μN for oocytes to 13 μN for embryos. The calculated embryo ZP elastic modulus is 42.2 kPa compared to 17.9 kPa for oocyte ZP. These ZP characterization results quantitatively describe mouse ZP mechanical properties and quantitate ZP hardening in postfertilization. The biomembrane force sensing technique and model presented in this paper can be applied to investigations into the mechanical properties of other biomembranes, such as the plasma membrane of oocytes or other cell types.

REFERENCES

[1] L. F. Liang, M. Familari, M. C. Moos, and J. Dean, "Coordinate expression of the three zona pellucida genes during mouse oogenesis," *Development*, vol. 121, pp. 1947–1956, 1995.

[2] G. Kania, "The structure properties and function of the zona pellucida of mammalian ovums," *Medcyna Weterynaryjna*, vol. 55, no. 5, pp. 295–299, 1999.

[3] A. C. Schroeder, R. M. Schultz, G. S. Kopf, F. R. Taylor, R. B. Becker, and J. J. Eppig, "Fetuin inhibits zona pellucida hardening and conversion of Zp2 to Zp2f during spontaneous mouse oocyte maturation in vitro in the absence of serum," *Biol. Reproduction*, vol. 43, no. 5, pp. 891–897, 1990.

[4] I. Demeestere, P. Barlow, and F. Leroy, "Hardening of zona pellucida of mouse oocytes and embryos in vivo and in vitro," *Int. J. Fertil. Womens Med.*, vol. 42, no. 3, pp. 219–222, 1997.

[5] Y. Sun, B. J. Nelson, D. P. Potasek, and E. Enikov, "A bulk microfabricated multi-axis capacitive cellular force sensor using transverse comb drives," *J. Micromech. Microeng.*, vol. 12, no. 6, pp. 832–840, 2002.

[6] B. Hogan, R. Beddington, F. Costantini, and E. Lacey, *Manipulating the Mouse Embryo: A Laboratory Manual*, 2nd ed. Woodbury, NY: Cold Spring Harbor Lab. Press, 1994.

[7] H. Hertz, "On the contact of elastic solids," *J. Reine Agnew. Math.*, vol. 92, pp. 156–171, 1881.

[8] K. L. Johnson, *Contact Mechanics*. Cambridge, U.K.: Cambridge Univ. Press, 1987.

[9] I. N. Sneddon, "The relationship between load and penetration in the axisymmetric boussinesq problem for a punch of arbitrary profile," *Int. J. Eng. Sci.*, vol. 3, pp. 47–57, 1965.

[10] D. Maugis, *Contact, Adhesion and Rupture of Elastic Solids*. New York: Springer-Verlag, 2000.

[11] J. M. Mitchison and M. M. Swann, "The mechanical properties of the cell surface: I. the cell elastimeter," *J. Exp. Biol.*, vol. 31, pp. 443–460, 1954.

[12] E. Evans and R. Skalak, *Mechanics and Thermodynamics of Biomembranes*. Boca Raton, FL: CRC, 1980.

[13] E. Evans and D. Needham, "Physical properties of surfactant bilayer membranes: Thermal transitions, elasticity, rigidity, cohesion, and colloidal interactions," *J. Phys. Chem.*, vol. 91, pp. 4219–4228, 1987.

[14] D. Needham and R. S. Nunn, "Elastic deformation and failure of lipid bilayer membranes containing cholesterol," *Biophys. J.*, vol. 58, pp. 997–1009, 1990.

[15] R. M. Hochmuth, "Micropipette aspiration of living cells," *J. Biomech.*, vol. 33, pp. 15–22, 2000.

[16] M. A. Haider and F. Guilak, "An axisymmetric boundary integral model for assessing elastic cell properties in the micropipette aspiration contact problem," *Trans. ASME*, vol. 124, pp. 586–595, 2002.

[17] K. T. Wan, V. Chan, and D. A. Dillard, "Constitutive equation for elastic indentation of a thin-walled bio-mimetic microcapsule by an atomic force microscope tip," *Colloids Surf. B: Biointerfaces*, vol. 27, pp. 241–248, 2002.

[18] K. T. Wan and K. K. Liu, "Contact mechanics of a thin-walled capsule adhered onto a rigid planar substrate," *Med. Biol. Eng. Comput.*, vol. 39, pp. 605–608, 2001.

[19] C. Dietrich, M. Angelova, and B. Pouligny, "Adhesion of latex spheres to giant phospholipid vesicles: Statics and dynamics," *J. Phys. II France*, vol. 7, pp. 1651–1682, 1997.

[20] A. Vinckier and G. Semenza, "Measuring elasticity of biological materials by atomic force microscopy," *FEBS Lett.*, vol. 430, pp. 12–16, 1998.

[21] J. Domke, S. Dannöhl, W. J. Parak, O. Müller, W. K. Aicher, and M. Radmacher, "Substrate dependent differences in morphology and elasticity of living osteoblasts investigated by atomic force microscopy," *Colloids Surf. B: Biointerfaces*, vol. 19, pp. 367–379, 2000.

[22] J. C. Bischof, W. F. Wolkers, N. M. Tsvetkova, A. E. Oliver, and J. H. Crowe, "Lipid and protein change due to freezing in dunning AT-1 cells," *Cryobiology*, vol. 45, no. 1, pp. 22–32, 2002.

[23] M. Radmacher, M. Fritz, C. M. Kacher, J. P. Cleveland, and P. K. Hansma, "Measuring the viscoelastic properties of human platelets with the atomic force microscope," *Biophys. J.*, vol. 70, pp. 556–567, 1996.

[24] A. L. Weisenhorn, M. Khorsandi, S. Kasas, V. Gotzos, and H. J. Butt, "Deformation and height anomaly of soft surfaces studied with an AFM," *Nanotechnology*, vol. 4, pp. 106–113, 1993.

[25] S. G. Shroff, D. R. Saner, and R. Lal, "Dynamic micromechanical properties of cultured rat atrial myocytes measured by atomic force microscopy," *Amer. J. Physiol.*, vol. 269, pp. 286–292, 1995.

[26] V. Parpura and J. M. Fernandez, "Atomic force microscopy study of the secretory granule lumen," *Biophys. J.*, vol. 71, pp. 2356–2366, 1996.

[27] R. P. Rand and A. C. Burton, "Mechanical properties of the red cell membrane. I. membrane stiffness and intracellular pressure," *Biophys. J.*, vol. 4, pp. 115–135, 1964.

[28] H. Huang, R. D. Kamm, P. T. C. So, and R. T. Lee, "Receptor-based differences in human aortic smooth muscle cell membrane stiffness," *Hypertension*, vol. 38, no. 5, pp. 1158–1161, 2001.

Kai-Tak Wan received the B.Sc. degree (1st Hon.) from University of New South Wales, Sydney, Australia, in 1988 and the Ph.D. degree in chemical physics from University of Maryland, College Park, in 1993.

He is currently Assistant Professor of Mechanical Engineering at University of Missouri, Rolla. His research focuses on mechanical and adhesion characterization of single cell, ultrathin biomembrane and multicell aggregates, and mechanics of stem cell condensation.

Kenneth P. Roberts received the Ph.D. degree in biochemistry from Washington State University, Pullman, in 1989.

He was a Postdoctoral Fellow at The Johns Hopkins University, Baltimore, MD. He is currently an Assistant Professor in the Department of Urologic Surgery, University of Minnesota, Minneapolis. His research interests are in the area of male reproductive biology, particularly sperm maturation and epididymal function, and sperm–egg interactions.

John C. Bischof received the B.S. degree in bioengineering from the University of California, Berkeley, in 1987, the M.S. degree from the University of California, Berkeley and San Francisco (joint program) in 1989, and the Ph.D. degree in mechanical engineering from the University of California, Berkeley, in 1992.

He was a Postdoctoral Fellow at Harvard University, Cambridge, MA. He is currently a Professor in the Department of Mechanical Engineering with joint appointments in Biomedical Engineering and Urologic Surgery at the University of Minnesota, Minneapolis. He has over 80 peer-reviewed publications and several patents filed or issued.

Dr. Bischof has received several Young Investigator and Best Paper awards in bioheat transfer.

Yu Sun (S'01–M'03) received the B.S. degree in electrical engineering from the Dalian University of Technology, Dalian, China, in 1996, the M.A. degree from the Institute of Automation, Chinese Academy of Sciences, Beijing, China, in 1999, and the Ph.D. degree in MEMS and microrobotics from the University of Minnesota, Minneapolis, in 2003.

He is currently a Postdoctoral Research Fellow at the Swiss Federal Institute of Technology (ETH) Zürich, Zürich. His research interests are in the areas of MEMS design, fabrication and testing, control of microstructures, microrobotics, biomechanics, microrobotic biological cell manipulation for biomedical applications, and nanofabrication and nanomanipulation.

Bradley J. Nelson (M'90) received the B.S. degree in mechanical engineering from the University of Illinois, Urbana, in 1984, the M.S. degree in mechanical engineering from the University of Minnesota, Minneapolis, in 1987, and the Ph.D. degree in robotics from the School of Computer Science, Carnegie Mellon University, Pittsburgh, PA, in 1995.

He has been on the faculty of the University of Minnesota and the University of Illinois, Chicago, has worked at Motorola and Honeywell, and has served as a U.S. Peace Corps Volunteer in Botswana, Africa. He is currently the Professor of Robotics and Intelligent Systems and heads the Institute of Robotics and Intelligent Systems (IRIS) at the Swiss Federal Institute of Technology (ETH) Zürich, Zürich.